Materials Science-Poland, 35(2), 2017, pp. 427-434
http://www.materialsscience.pwr.wroc.pl/
DOI: 10.1515/msp-2017-0040

DE GRUYTER OPEN

Synthesis of Cu and Ce co-doped ZnO nanoparticles: crystallographic, optical, molecular, morphological and magnetic studies

MOHIT RAWAT[1,*], JASMEET SINGH[1], JAGPREET SINGH[1], CHAMKAUR SINGH[1], AMRITPAL SINGH[1], DEEPAK KUKKAR[1], SANJEEV KUMAR[2]

[1]Department of Nanotechnology, Sri Guru Granth Sahib World University, Fatehgarh Sahib, Punjab 140406, India
[2]Department of Physics, Sri Guru Granth Sahib World University, Fatehgarh Sahib, Punjab 140406, India

In the present research work, crystallographic, optical, molecular, morphological and magnetic properties of $Zn_{1-x}Cu_xO$ (ZnCu) and $Zn_{1-x-y}Ce_yCu_xO$ (ZnCeCu) nanoparticles have been investigated. Polyvinyl alcohol (PVA) coated ZnCu and ZnCeCu nanoparticles have been synthesized by chemical sol-gel method and thoroughly studied using various characterization techniques. X-ray diffraction pattern indicates the wurtzite structure of the synthesized ZnCu and ZnCeCu particles. Transmission electron microscopy analysis shows that the synthesized ZnCu and ZnCeCu particles are of spherical shape, having average sizes of 27 nm and 23 nm, respectively. The incorporation of Cu and Ce in the ZnO lattice has been confirmed through Fourier transform infrared spectroscopy. Room temperature photoluminescence spectra of the ZnO doped with Cu and co-doped Ce display two emission bands, predominant ultra-violet near-band edge emission at 409.9 nm (3 eV) and a weak green-yellow emission at 432.65 nm (2.27 eV). Room temperature magnetic study confirms the diamagnetic behavior of ZnCu and ferromagnetic behavior of ZnCeCu.

Keywords: *copper and cerium co-doped ZnO; wurtzite structure; transmission electron microscope; magnetization; optical properties*

1. Introduction

In recent years, one-dimensional (1D) nanostructures like nanowires, nanorods, nanobelts and nanotubes have attracted a great deal of interest in academic as well as industrial research [1, 2]. These nanostructures find applications in electronic devices and circuits, optoelectronic integrated circuits, electrochemical and electromechanical devices, etc. [3, 4]. Over the last decade, considerable attempts have been made for the development of various 1D semiconductor nanostructures with emphasis on III-V, and II-VI semiconductor compounds. Among various semiconductor compounds, zinc oxide (ZnO) is considered to be one of the most important nanomaterials due to its superior optoelectronic and magnetic properties [5]. ZnO is a direct wide band gap material ($E_g \sim 3.3$ eV at 300 K) in near-UV region [6–10]. Its large free exciton binding energy (60 meV) allows efficient excitonic emission over UV and visible region at room temperature [11, 12]. Some optoelectronic properties of ZnO overlap with that of wurtzite gallium nitride (GaN; $E_g \sim 3.4$ eV at 300 K, 21 meV to 25 meV, widely used for production of green, blue, and white light emitting devices). As compared to GaN, only high purity large size single crystals of ZnO can be grown at laboratory as well industrial level. This might be due to the single crystal growth manufacturing technology only realized in ZnO, whereas it has never been available for GaN and other materials [11]. The development of electronic industry started with availability of wide gap semiconductor materials like germanium, silicon, gallium nitride [12]. Consequently, the need of newer wide gap semiconductor materials with high purity, large size single crystals has become apparent. This has

*E-mail: mohitnano.nit@gmail.com

led to an accelerating scientific interest in ZnO in electronic industry [13]. Other significant properties of ZnO material, due to which it exhibits interesting application in biomedical and textile industries is biocompatibility and biosafety [14, 15]. ZnO nanostructures doped with a small amount of magnetic impurities are among the most interesting new class of magnetic materials which find potential application in spintronics. The main challenge for any material to be utilized for spintronic application is to exhibit a Curie temperature above 300 K. ZnO doped with certain transition metal ions displays Curie temperature above 300 K, hence enabling its efficient application in spintronics [16, 17]. For spintronics applications, Sharma et al. [18], in 2003 confirmed the ferromagnetic behavior of ZnO when doped with Mn. Dopant which is not properly incorporated to the ZnO lattice, leads to the formation of secondary phase. This is one of the main obstacles in creating ferromagnetism in ZnO [19, 20]. The recent work by Costa-Kramer et al. [19], Garcia et al. [20], and Liu et al. [21], also confirmed that presence of magnetic ions is not exclusively responsible for the magnetic properties of ZnO; it is also strongly determined by defects in ZnO.

In the present research work, structural, optical, photoluminescence and magnetic properties of $Zn_{1-x}Cu_xO$ and $Zn_{1-x-y}Ce_yCu_xO$ ($x = 0.05$ and $y = 0.04$) nanoparticles coated with polyvinyl alcohol (PVA) have been investigated. The PVA coated particles were synthesized by sol-gel method and characterized by XRD, TEM, FT-IR, PL and VSM.

2. Materials and methods

2.1. Materials

Zinc acetate [$(CH_3COO)_2Zn{\cdot}2H_2O$], copper chloride ($CuCl_2{\cdot}6H_2O$) and cerium chloride ($CeCl_3{\cdot}2H_2O$), polyvinyl alcohol $(C_2H_4O)_n$, ethanol (C_2H_6O) and acetic acid ($C_2H_4O_2$) were purchased from Merck Germany. All the glass wares were rinsed with concentrated HNO_3 and distilled water and dried in an oven. Type-I deionized (DI) water (Siemens, Singapore) was used in all the experiments wherever required.

2.2. Preparation of $Zn_{1-x}Cu_xO$ (ZnCu) and $Zn_{1-x-y}Ce_yCu_xO$ (ZnCeCu) nanostructures

For the synthesis of ZnO, doped with copper (Cu) and co-doped with cerium (Ce), well-known chemical sol-gel method has been used [22, 23]. In a typical experimental process, desired molar ratio of precursor solutions were prepared from zinc acetate [$(CH_3COO)_2Zn{\cdot}2H_2O$], copper chloride ($CuCl_2{\cdot}6H_2O$) and cerium chloride ($CeCl_3{\cdot}2H_2O$). Polyvinyl alcohol (PVA) was used as a stabilizing agent for ZnO particles. Ethanol (C_2H_6O) and acetic acid ($C_2H_4O_2$) were mixed in the ratio of 3:1. Zinc acetate solution was added to it and stirred for two hours. In this solution, dopant Cu and co-dopant Ce were added in the desired stoichiometric ratio and stirred for another one hour. Further, to this molar solution (M), PVA was added in the molar ratio of M:PVA = 5:2. The reaction was completed with formation of precipitates. For the complete crystallization of precipitates, the solution was dried at 250 °C and annealed at 700 °C for two hours.

2.3. Characterization

The phase purity and crystal structure of the synthesized samples were determined from X-ray diffraction patterns recorded using X-ray diffractometer (PANalytical X'Pert Pro) with CuKα radiation source (1.542 Å). The size and morphology of nanoparticles were determined using transmission electron microscope (H-7500, Hitachi) operated at an acceleration voltage of 100 kV. Photoluminescence (PL) spectra of the Cu and Ce doped ZnO nanoparticles were recorded using a spectrofluorometer (Cary Eclipse, Varian). Surface stabilization of ZnO by PVA and incorporation of Cu and Ce into the ZnO lattice were analyzed using Fourier transform infrared (FT-IR) spectrometer (BX II, PerkinElmer). Magnetic behavior of ZnO doped with Cu and Ce were analyzed using vibrating sample magnetometer (7307, Lakeshore).

3. Results and discussion

3.0.1. Phase and structural analysis of ZnCu and ZnCeCu

X-ray diffraction patterns of ZnO doped with Cu and co-doped with Ce, annealed at 700 °C for two hours have been shown in Fig. 1. The prominent X-ray diffraction lines in the diffractogram correspond to (1 0 0), (0 0 2), (1 0 1), (1 0 2) and (1 1 0) reflection planes of ZnO as observed at 2θ values of 31.8, 34.6, 36.3, 47.6 and 56.7, respectively. On comparison with standard ZnO sample (JCPDS# 5-664) [14], the X-ray diffractograms and 2θ values of synthesized ZnO were found to be in fairly good agreement, thus confirming the hexagonal wurtzite phase of ZnO with a space group $P6_3mc$ for all samples.

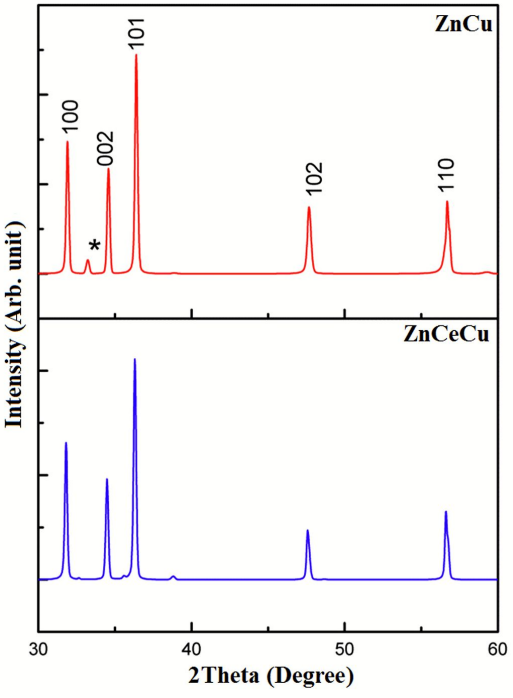

Fig. 1. XRD pattern on ZnCu and ZnCeCu.

Lattice parameters for hexagonal wurtzite ZnO structure have been calculated using the following equations [24]:

$$\frac{1}{d^2} = \frac{4}{3}\left(\frac{h^2+hk+k^2}{a^2}\right) + \frac{l^2}{c^2} \qquad (1)$$

$$\lambda = 2d\sin\theta \qquad (2)$$

where d is the spacing between lattice planes, a and c are lattice parameters, θ is the diffraction angle, λ is the incident wavelength; h, k and l are the Miller indices. Based on the whole spectra fitting method, the values of lattice parameters, i.e. a and c and crystallite size have been calculated and given in Table 1.

3.1. Morphological analysis ZnCu and ZnCeCu nanostructures

Fig. 2 and Fig. 3 show the high magnification and resolution images of ZnO doped with Cu and co-doped with Ce, taken with a transmission electron microscope (TEM). Fig. 2a shows the non-agglomerated particles with consistent shapes. Each spherical cloud consists of three to four particles. The nanometer bar scale in the TEM image confirms the nanometer size of the synthesized ZnO particles. Fig. 2b shows the histogram of size distribution for ZnCu nanoparticles.

The average size of synthesized particles has been calculated from TEM micrograph by plotting a histogram, and was found to be 27 nm for ZnCu. Fig. 3a also shows the bunch of non-agglomerated particles with consistent shapes. Each spherical cloud consists of four to six particles. The nanometer bar scale in the TEM image confirms the nanometer size of the synthesized ZnCeCu particles. Fig. 3b shows the histogram of size distribution of ZnCeCu nanoparticles. The average size of ZnCeCu particles has been calculated from TEM micrographs by plotting the histogram, and was found to be 23 nm.

Similar type of morphology and sizes of ZnO nanoparticles have also been observed by Pal et al. [25]. The values of average diameter (d) and length (l) of each particle have been given in Table 1.

3.2. FT-IR analysis of ZnCu and ZnCeCu particles

The Fourier transform infrared (FT-IR) spectra of ZnCu and ZnCeCu have been shown in Fig. 4 and Fig. 5, respectively. The spectra were

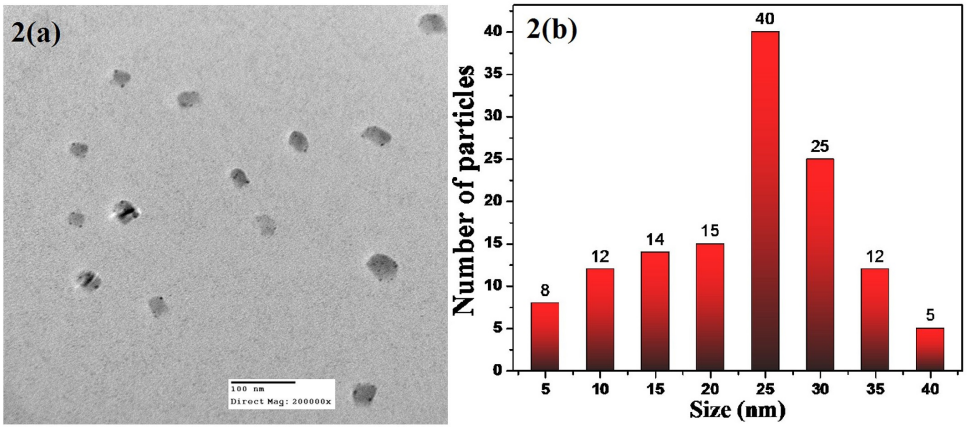

Fig. 2. TEM image of (a) ZnCu particles and (b) size distribution.

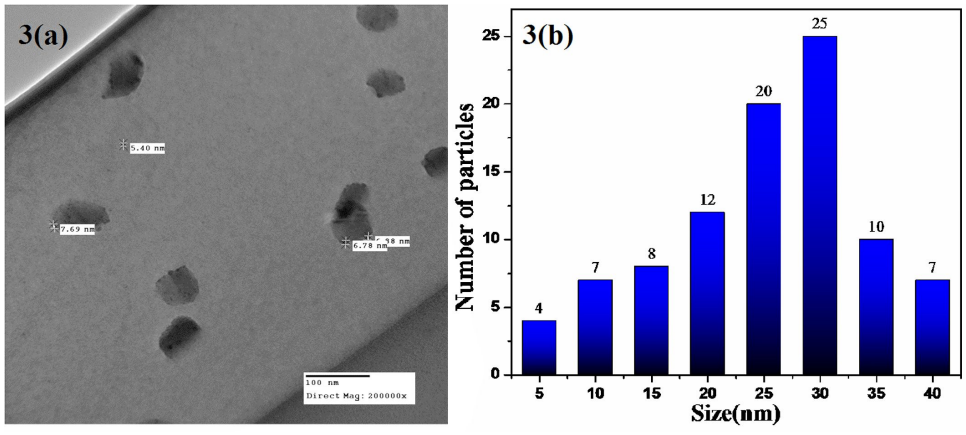

Fig. 3. TEM image of (a) ZnCeCu particles and (b) size distribution.

recorded in the transmittance mode and were used to study various bands of Zn–O. In the absorption spectra (Fig. 4) of Cu doped ZnO, a number of absorption peaks can be observed. The wave number at 677.23 cm^{-1} is attributed to C–H bending of alkynes, 1233.62 cm^{-1} corresponds to vibrations of C–N stretching of aliphatic amines, 1587.34 cm^{-1} corresponds to C–C stretching of aromatics, 2338.15 cm^{-1} corresponds to C≡N stretching of nitriles and 3638.97 cm^{-1} corresponds to vibrations from O–H stretching of alcohols and phenols. Similarly, in the absorption spectra of Cu doped and Ce co-doped ZnO (Fig. 5), we can observe the absorption peaks at wave number 656.26 cm^{-1} attributed to C–Br stretching of alkyl halides, 1226.56 cm^{-1} corresponding to vibrations of C–N stretching of aliphatic amines, 1698.34 cm^{-1} corresponding to C=O stretching of aldehydes and ketones, 2352.78 cm^{-1} corresponding to C≡N stretching of nitriles and 3151.77 cm^{-1} corresponding to vibrations of C–N stretching of aromatics. The bands in the range of 600 cm^{-1} to 800 cm^{-1} are attributed to the vibration of Zn–O–Cu and Ce bonds, respectively. The vibrations of usual bands of ZnO have been changed due to presence of Cu and Ce. This also confirms that Cu and Ce are well incorporated in the ZnO lattice.

3.3. PL study of ZnCu and ZnCeCu nanostructures

Fig. 6 and Fig. 7 show the photoluminescence spectra of ZnCu and ZnCeCu samples

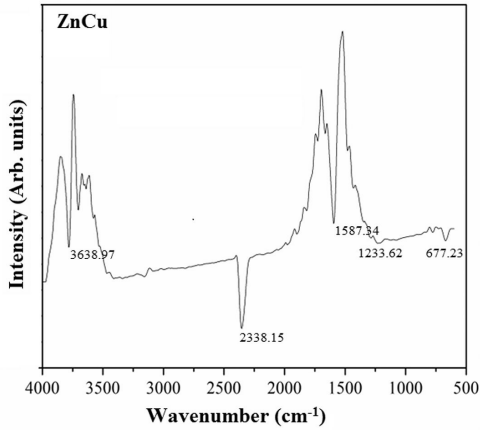

Fig. 4. FT-IR spectra of ZnCu particles.

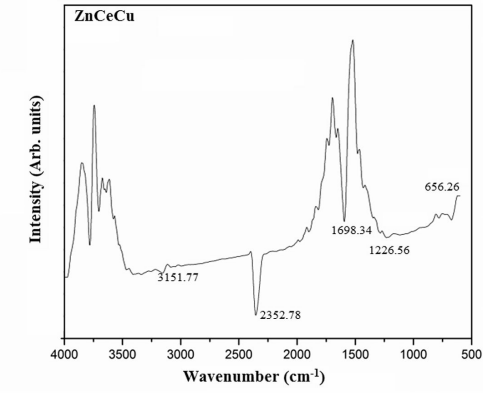

Fig. 5. FT-IR spectra of ZnCeCu particles.

(annealed at 700 °C) at an excitation wavelength of 325 nm (3.81 eV). It shows an ultraviolet (UV) near-band edge emission at 409.9 nm (3 eV) and a broad green-yellow emission around 430.22 nm (2.27 eV). UV emission in the samples might be due to the recombination of free excitons through an exciton-exciton collision process [26] as well as transitions of excited optical centers from the deep level to the valence level (deep-level emissions are usually accompanied by the presence of structural defects and impurities). Green emission in ZnCu and ZnCeCu are caused by zinc interstitials, oxygen vacancies [26] and presence of singly ionized vacancies. Panigrahy et al. [27] proposed that the intensity of the green-yellow emission decreases after annealing the samples in oxygen rich environment.

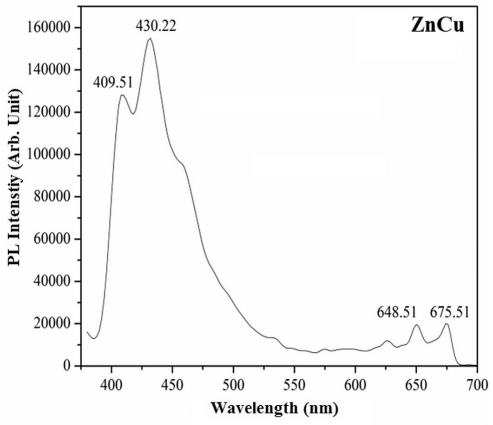

Fig. 6. PL spectra of ZnCu.

In the present research work, annealing of samples has been carried out at high temperatures (>700 °C) which led to the variation in the concentration of defects, such as oxygen vacancy and zinc vacancy as compared to unannealed samples. Thermal diffusion process is mainly responsible for this phenomenon and due to this, more deep level defects are created. These deep level defect bands compete with the UV emission which further decreases UV emission intensity in ZnO.

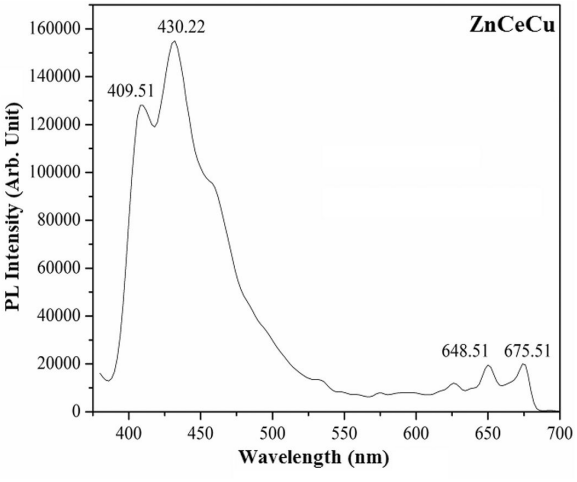

Fig. 7. PL spectra of ZnCeCu.

After the sample annealing, UV emission intensity depends upon two competing processes: recombination on the centers near the surface, which increases UV emission intensity and the formation of deep level defects which reduces the UV

emission intensity. Therefore, the structural and optical properties can be modified by the sample annealing.

3.4. M-H study of ZnCu and ZnCeCu

Fig. 8 and Fig. 9 show the magnetization (M) versus applied magnetic field (H), i.e. hysteresis curves (M-H) for ZnCu and ZnCeCu samples respectively at room temperature. M-H curves (Fig. 8) show that ZnCu exhibits diamagnetic behavior whereas ZnCeCu sample (Fig. 9) displays ferromagnetic behavior. The values of M_s calculated from Fig. 8 and Fig. 9 are 0.0023 emu/g and 0.01318 emu/g for ZnCu and ZnCeCu samples, respectively (Table 1). Magnetic nanostructures are commonly characterized by a high value of saturation magnetization (M_s). The variations in the values of M_s depend on various factors, such as the shape and size of nanostructures, their stoichiometric ratio, concentration of dopants, lattice parameters, etc. The ferromagnetic interaction mechanism mainly includes two effects: the Ruderman-Kittel-Kasuya-Yosida (RKKY) mechanism [28–31] and Bound Magnetic Polarons (BPM) formation [32]. RKKY is caused by the interaction of electronic spin of homogenously distributed dopant within the host materials whereas the formation of BMP is caused by the alignment of the spins in transition metal ions with those of weakly bound carriers (excitons within a polaron radius). The localized holes of the polarons act on the transition-metal impurities, leading to the production of an effective magnetic field by aligning all spins. The BMP model is inherently attractive for low carrier density systems such as ZnO.

M-H loop of ZnO doped with Cu (Fig. 8) shows the non-linear magnetic behavior of the compound. It confirms the diamagnetic nature of ZnCu with high value of coercive force around the origin. The value of coercive field (H_c) has been found to be 1497 Oe for ZnCu (Table 1). Similarly, M-H loop of ZnCeCu (Fig. 9) shows the nearly linear behavior of the compound. It confirms the ferromagnetic nature of the ZnO doped with Cu and co-doped with Ce, with low value of coercive force around

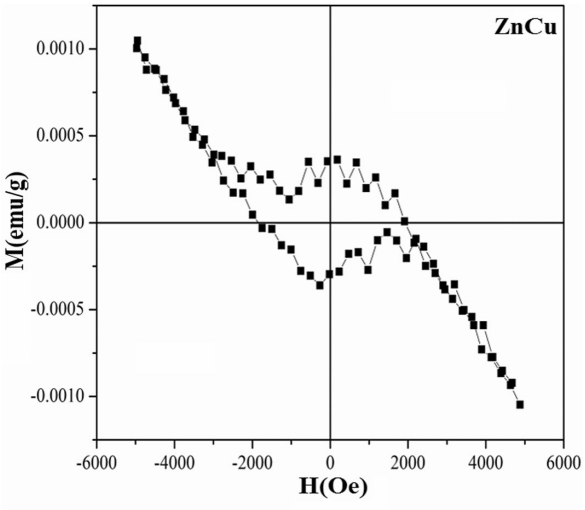

Fig. 8. M-H hysteresis of ZnCu.

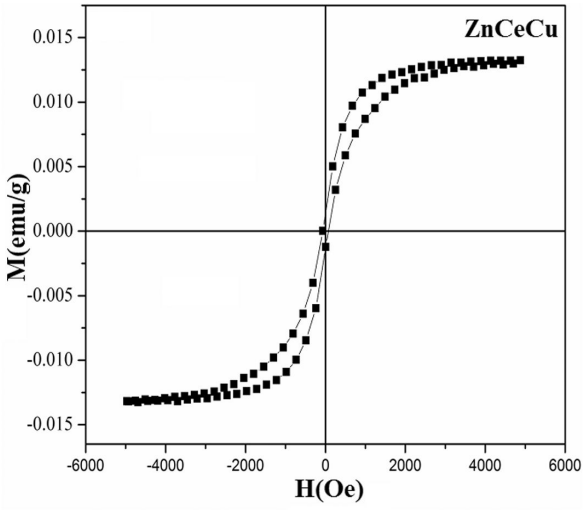

Fig. 9. M-H hysteresis of ZnCeCu.

the origin. The value of H_c has been found to be 44 Oe for ZnCeCu (Table 1). The small value of H_c shows the overlapping around the origin in the M-H loop as explained on the basis of both size dependent as well as magnetic behavior of dopants Cu and Ce in ZnO.

Generally, in ferromagnetic materials, assemblies of single-domain nanoparticles show different types of magnetic behavior depending on their interparticle distances. In recent years much experimental and theoretical work has been carried out to understand the interactions between the dopants and host materials [33].

Table 1. Values of Cu doped and Ce co-doped ZnO nanoparticles: lattice parameters (a and c), average particles size (x) from XRD, (x') from TEM, remanent magnetization (M_r), coercive field (H_c) and saturation magnetization (M_s).

Sample	ZnCu	ZnCeCu
a [Å]	3.24	3.23
c [Å]	5.19	5.18
x [nm]	14.46	11.9
x' [nm]	27	23
H_c [Oe]	1497	44
M_r [emu/g]	2.3	3.8
M_s [emu/g]	0.0023	0.01318

4. Conclusions

Copper doped and cerium co-doped ZnO nanoparticles have been successfully synthesized by sol-gel method using PVA as surfactant. The XRD pattern reveals the hexagonal wurtzite structure of the samples. TEM images show the average particle diameter of 27 nm and 23 nm, for ZnCu and ZnCeCu, respectively. FT-IR study confirms the effective incorporation of Ce and Cu in the ZnO lattice. PL spectra show UV near-band edge emission at 409.9 nm (∼3 eV) and a broad green-yellow emission band around 432.65 nm (∼2.27 eV). M-H curves show that ZnCu exhibits diamagnetic behavior whereas ZnCeCu sample exhibits ferromagnetic behavior. The saturation value of magnetization (M_s) for ZnCu and ZnCeCu has been found to be 0.0023 emu/g and 0.01318 emu/g, respectively. Small size of the synthesized particle might be the reason for higher values of M_s in ZnCuCe as compared to ZnCu. Therefore, the synthesized particles may find wide applications in optoelectronics as well as spintronics in future.

Acknowledgements

The authors are thankful to Vice Chancellor, the SGGSW University, Fatehgarh Sahib, India, for kind motivation and support.

References

[1] LOOK D.C., *Mater. Sci. Eng. B*, 80 (2001), 383.
[2] OZGUR U., ALIVOV Y.I., LIU C., TEKE A., RESHCHIKOV M.A., DOGAN S., AVRUTIN V., CHO S.J., MORKOC H., *J. Appl. Phys.*, 98 (2005), 041301.
[3] OGALE S.B., *Thin Films and Heterostructures for Oxide Electronics*, Springer, New York, 2005.
[4] NICKEL N.H., TERUKOV E. (Eds.), *Zinc Oxide – A Material for Micro and Optoelectronic Applications*, Springer, Netherlands, 2005.
[5] JAGADISH C., PEARTON S.J. (Eds.), *Zinc Oxide Bulk, Thin Films, and Nanostructures*, Elsevier, New York, 2006.
[6] THOMAS D.G., *J. Phys. Chem. Solids*, 15 (1960), 86.
[7] MANG A., REIMANN K., RUBENACKE S., *Solid State Commun.*, 94 (1995), 251.
[8] REYNOLDS D.C., LOOK D.C., JOGAI B., LITTON C.W., CANTWELL G., HARSCH W.C., *Phys. Rev. B*, 60 (1999), 2340.
[9] CHEN Y., BAGNALL D.M., KOH H.J., PARK K.T., HIRAGA K., ZHU Z.Q., YAO T., *J. Appl. Phys.*, 84 (1998), 3912.
[10] SRIKANT V., CLARKE D.R., *J. Appl. Phys.*, 83 (1998), 5447.
[11] REYNOLDS D.C., LOOK D.C., JOGAI B., *Solid State Commun.*, 99 (1996), 873.
[12] BAGNALL D.M., CHEN Y.F., ZHU Z., YAO T., KOYAMA S., SHEN M.Y., GOTO T., *Appl. Phys. Lett.*, 70 (1997), 2230.
[13] BROWN M.E. (Ed.), *ZnO – Rediscovered*, The New Jersey Zinc Company, New York, 1957.
[14] YI G.C., WANG C., PARK W.I., *Semicond. Sci. Technol.*, 20 (2005), S22.
[15] WANG Z. L., *J. Phys.Condens. Matter*, 16 (2004), R829.
[16] DIETL T., OHNO H., MATSUKURA F., CIBERT J., FERRAND D., *Science*, 287 (2000), 1019.
[17] SATO K., KATAYAMA-YOSHIDA H., *Physica E*, 10 (2001), 251.
[18] SHARMA P., GUPTA A., RAO K.V., OWENS F.J, SHARMA R., AHUJA R.,GUILLEN J.M.O., JOHANSSON B., GEHRING G.A.,*Nat.Mater.*, 2 (2003), 673.
[19] COSTA-KRAMER J.L., BRIONES F., FERNANDEZ J.F., CABALLERO A.C., VILLEGAS M., DIAZ M., GARCIA M.A., HERNANDO A., *Nanotechnology*, 16 (2005), 214.
[20] GARCIA M.A., RUIZ-GONZALEZ M.L., QUESADA A., COSTA-KRAMER J.L., FERNANDEZ J.F., KHATIB S.J., WENNBERG A., CABALLERO A.C., MARTÍN-GONZÁLEZ M. S., VILLEGAS M., BRIONES F., GONZALEZ-CALBET J.M., HERNANDO A., *Phys. Rev. Lett.*, 94 (2005), 217206.
[21] LIU C., YUN F., MORKOC H., *J. Mater. Sci. Mater. Electron.*, 16 (2005), 555.
[22] FU M., LI Y., WU S., LU P., LIU J., DONG F., *Appl. Surf. Sci.*, 258 (2011), 11591.
[23] CHEN X., *Chem. Rev.* 10 (2009), 2891.
[24] ZAK A.K., MAJID W.H.A., ABRISHAMIA M.E., YOUSEFI R., *Solid State Sci.*, 13 (2011), 251.
[25] PAL B., GIRI P.K., *J. Appl. Phys.*, 108 (2010), 084322.
[26] UMA K., ANANTHAKUMAR S., MANGALARAJA R.V., MAHESH K.P.O., SOGA T., JIMBO T., *J. Sol-Gel Sci. Technol.*, 49 (2009), 1.

[27] PANIGRAHY B., ASLAM M., MISRA D.S., GHOSHAND M., BAHADUR D., *Adv. Funct. Mater.*, 20 (2010), 1161.
[28] ZHOU L., WIEBE J., LOUNIS S., VEDMEDENKO E., MEIER F., BLUGEL S., DEDERICHS P.H., WIESENDANGER R., *Nat. Phys.*, 6 (2010), 187.
[29] DJERDJ I., JAGLICIC Z., ARCON D., NIEDERBERGER M., *Nanoscale*, 2 (2010), 1096.
[30] SALEEM M., SIDDIQI S.A., RAMAY S.M., ATIQ S., NASEEM S., *Chin. Phys. Lett.*, 29 (2012), 106103.
[31] BELOKON V.I., NEFEDEV K.V., KAPITAN V.Y., DYACHENKO O.I., *Adv. Mat. Res.*, 774 (2013), 523.
[32] BEDNARSKI H., SPALEK J., *J. Phys. Condens. Matter*, 24 (2012), 235801.
[33] LIEBER C.M., WANG Z.L., *MRS Bull.*, 32 (2007), 99.

Received 2016-11-12
Accepted 2017-02-10